Critical dimension metrology using Optical Diffraction Microscopy

Niels Agersnap[a], Poul-Erik Hansen[a*], Jan Conrad Petersen[b], Jørgen Garnæs[b], Nathalie Destouches[c], Olivier Parriaux[c]
[a]LuKa OptoScope, Rørmose Parkvej 50, DK-3520 Farum, Denmark;
[b]Danish Fundamental Metrology, Matematiktorvet 307, DK-2800 Kgs. Lyngby, Denmark;
[c]University of Saint-Etienne, Laboratoire TSI
Campus du Pôle Optique et Vision - Bâtiment F, 18 rue Benoît Lauras, F-42000 Saint-Etienne, France

ABSTRACT

We present an innovative method Optical Diffraction Microscopy (ODM). for the simultaneous measurement of specular and non-specular diffraction patterns of sub-micron periodic structures. A sample is illuminated with broadband light and the diffraction pattern is collected by using a pair of ellipsoidal mirrors, optical fibers and a spectrometer. This method allows for rapid measurements and makes used of the Rigorous Coupled Wave algorithm for data analysis. In the present work the method has been applied to binary and multi-layer sub-micron gratings. A series of binary gratings with periods of 318 nm and 360 nm with different exposure levels of the photoresist were investigated. We succeded in characterize underexposed, ideally exposed and overexposed photoresist grating profiles. The measurements are well-suited to determine the delivered exposure energy density to photoresist gratings. The ODM technique may thus be applied to specify the exposure window and as a feedback in order to adjust the exposure energy density on-line. The homogeneity of a grating on multi-layered substrate has been investigated. Heights and duty cycles ranging from 50 nm to 55 nm and 0.25 to 0.97, respectively, have been found. AFM measurements of the gratings verify the ODM results and demonstrate that the ODM technique can be used to determine grating topology.

Keywords: Critical dimension, optical metrology, novel testing technique, gratings

1. INTRODUCTION

Traditional techniques based on scalar diffraction have been used to assess the topography of surfaces from the diffraction patterns. However, scalar diffraction theory, especially in the paraxial approximation, has limited feature size resolution[1,2]. The work by Pommet *et al* showed that the period to wavelength ratio should be approximately 15 to resolve one-dimensional lamellar dielectric gratings. Korner *et al*[3] used scalar analysis to study the interferograms of lamellar and trapezoidal one-dimensional gratings and found that the ratio could be extended down to 10. Scatterometry is a recent optical technique that is capable of measuring sub-micron gratings. Measurements are performed in a specular configuration at a fixed incident angle for a range of wavelengths. The measuring geometry makes it difficult to detect the asymmetry of the grating profile. Additionally the bottom of the cross-sectional grating profile is difficult to measure accurately due to screening effects.

We present an ODM system that overcomes these shortcomings[4]. The system reconstructs the profile of asymmetric gratings from a single measurement at minimal computational burden. The experimental setup records the diffracted wavelength spectrum and diffracted angles simultaneously for a given incident angle and polarization mode. The recover of the grating profile from the measured diffraction data is performed using an inversion algorithm based on the Rigorous Coupled Wave (RCW) method and pre-calculated diffraction intensities.

* peh@lukaoptoscope.com; phone +45 4494 5852; URL: http://www.lukaoptoscope.com

The capability of the ODM technique is demonstrated by performing measurements on two types of gratings. The examples will show that the ODM is capable of:

- Achieving accurate quantitative values such as height, duty cycle and effective duty cycle of grating profiles
- Detecting exposure level variations in printing gratings, which leads to complete or non-complete removal of resist between the grating lines
- Grating homogeneity measurement on multi-layered grating structure

The first type of gratings is manufactured using near-field holography (NFH) printing technique where exposure densities ranging from underexposed to overexposed levels have been applied. The second type is a multi-layer diffraction (MLD) grating structure comprising alternating layers of Ta_2O_5 and SiO_2 deposited by ion plating where the outer Ta_2O_5 layer is being corrugated.

The ODM measurements are verified with Atomic Force Microscopy (AFM) measurements through quantitative comparisons of the grating profile parameters.

2. OPTICAL DIFFRACTION MICROSCOPE

Optical interaction with periodic structures is well-known to generate diffraction patterns that are strongly dependent on the geometry and material properties of the repeating profile of the structure.
This unique relation between the diffraction pattern and the repeated structure is applied to reconstruct the arbitrary cross-sectional profile from quantities including angle of incidence, polarization mode, wavelength and diffraction efficiency. An illustrative implication of the property of diffracted light from periodic structures is that symmetric profiles generate equal magnitude of conjugated diffraction efficiencies of negative and positive orders for normal incident illumination while asymmetric structures have unequal magnitude of conjugated negative and positive efficiencies.

2.1. The principle of the Optical Diffraction Microscopy

The ODM apparatus[4] for measuring transmission diffraction efficiency is sketched in Figure 1. The sample is illuminated by a broad continuous light spectrum provided by a deuterium-halogen lamp. The light is shaped by a collimator, polarizer and aperture before entering the sample at normal incidence.
The diffracted beams are collected by a reflector-based system that focuses the light, without chromatic aberrations, into two fibers. The reflector-based system consists of an ellipsoidal mirror divided into two counterparts and tilted such that their focal points are spatially separated and thereby enables simultaneous collection of both the negative (-) and the positive (+) diffracted orders into fibers situated at the focal points. The transmitted zero-order beam propagates between the mirror counterparts and is collected by a third fiber (0). The range of collected diffraction angles by the mirrors is from 2° to 88°. The diffraction intensity are via fibers and an optical switch box detected by a spectrometer.

The zero-order diffraction efficiency η_0 may be obtained by normalization of the measured diffracted intensity with the intensity of the direct light entering fiber 0. A representation of the high-order diffraction signals is achieved by introducing the ratio between the positive and negative diffraction intensities.
The measured zero-order diffraction efficiency η_0 is found as the ratio between the grating signal $I_{grating}$ subtracted the background signal $I_{background}$ and the reference signal I_{ref} subtracted the same background signal, i.e.

$$\eta_0 = \frac{I_{grating} - I_{background}}{I_{ref} - I_{background}}.$$

Similarly the measured ratio between positive and negative diffraction orders is determined by following expression

$$\eta_{ratio} = \frac{\sum_{m>0} I_{grating} - I_{background}}{\sum_{m<0} I_{grating} - I_{background}} = \frac{I^{+}_{grating} - I_{background}}{I^{-}_{grating} - I_{background}}.$$

The ODM reconstruction of the grating profile is based on the recorded zero-order diffraction efficiency spectrum $\boldsymbol{\eta}_0 = \{\eta_0(\lambda_1), \eta_0(\lambda_2), ..., \eta_0(\lambda_n)\}$ and high-order efficiency ratio spectra $\boldsymbol{\eta}_{ratio} = \{\eta_{ratio}(\lambda_1), \eta_{ratio}(\lambda_2), ..., \eta_{ratio}(\lambda_n)\}$.

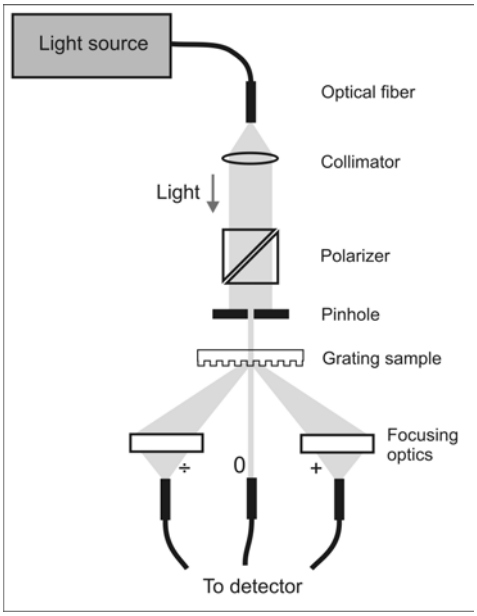

Figure 1: Schematic of the ODM setup in transmission mode.

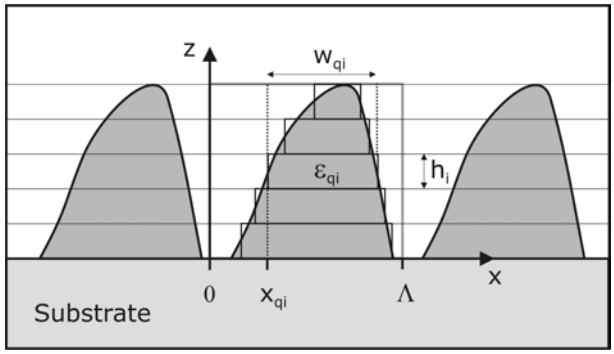

Figure 2: The diffractive efficiencies generated from a grating are calculated from a multi-level approximation of the profile by slabs of width w_{qi}, height h_{qi} and displacement x_{qi}.

2.2. Analysis

Using the measured and normalized diffraction intensities together with a seed profile, an algorithm analyses the data in the following manner[5]. A database of seed profiles is accessed and searched for a match to the measured data. The database consists of normalized diffraction intensities for series of profiles that are calculated using the Fourier modal method[6,7,8].

An arbitrary profile of the repeated structure, sketched in Figure 2, is approximated by descretization into multi-level slabs. Slab i is composed of building blocks labeled with a lateral and vertical index (q,i) and characterized by its width w_{qi}, offset x_{qi} in the lateral direction, height h_i and index of refraction n_{qi}. In addition to the geometrical and material quantities the model calculation requires the electromagnetic parameters of the incoming light represented by plane waves: wavelength λ, polarization mode, and the direction of propagation given by the incident angle θ and azimuth angle ϕ.

Each seed model is parameterized such that the geometrical shape of the cross-sectional profile along the repeated direction x is represented by a continuous profile function $z(x, \boldsymbol{\alpha})$ with the adjustable parameters contained in the vector $\boldsymbol{\alpha} = (\alpha_1, ..., \alpha_u)$. An example of a profile function is the symmetrical trapezoidal profile characterized by the parameters, profile height α_1, profile width α_2, profile side wall angle α_3 and period α_4 in the repeated direction x.
We have implemented a wide range of photoresist and etch profiles including symmetrical and asymmetrical trapezoidal as well as stacked symmetrical and asymmetrical trapezoidal. The database applied to identify the optimal lookup table in the reconstruction consists of modeled data arrays for various profiles. Each data array represents tabulated diffraction efficiencies $\boldsymbol{\eta}_0^{theory}$ and ratio between diffraction efficiencies $\boldsymbol{\eta}_{ratio}^{theory}$ of carefully pre-defined values of wavelength, angle of incidence and polarization mode.

The searching technique used to select the seed model in the database is based on the least-square error approach by minimizing the total sum of squares of the difference between the measured and modeled efficiencies of the seed model.
We use the reduced chi-squared χ^2 as measure for the goodness of the match. The reduced χ^2 is expressed as

$$\chi^2 = \frac{1}{N}\sum_{i=1}^{N}\left(\frac{\eta_i - \eta^{theory}(\Omega_i, \boldsymbol{\alpha})}{\sigma_i}\right)^2 \tag{1}$$

where N is the number of measured efficiency data points and $\Omega_i = \{\theta_i, \lambda_i, ...\}$ represents the pre-defined values of incident angle θ, wavelength λ, polarization mode, etc.
We have merged the spectra of the zero-order diffraction efficiency and high-order efficiency ratio into a single vector, i.e. for measured data $\boldsymbol{\eta} = [\boldsymbol{\eta}_0, f\boldsymbol{\eta}_{ratio}]$ and modeled $\boldsymbol{\eta}^{theory} = [\boldsymbol{\eta}_0^{theory}, f\boldsymbol{\eta}_{ratio}^{theory}]$. The factor f is applied to adjust the data vectors $\boldsymbol{\eta}_0$ and $\boldsymbol{\eta}_{ratio}$ to have equal χ^2-weight.

Similar the standard uncertainty, that is required to obtain the reduced χ^2, is written as $\boldsymbol{\sigma} = [\boldsymbol{\sigma}_0, \boldsymbol{\sigma}_{ratio}]$ where $\boldsymbol{\sigma}_0$ and $\boldsymbol{\sigma}_{ratio}$ are the standard uncertainty vectors for zero-order diffraction efficiency data points and high-order efficiency ratio data points, respectively.
The standard uncertainty vector $\boldsymbol{\sigma}$ is determined by use of the propagation of error formula applied to the expressions of $\boldsymbol{\eta}_0$ and $\boldsymbol{\eta}_{ratio}$ which depends on the photon count value of the measured intensities $\mathbf{I}_{grating}$, $\mathbf{I}_{ref}$ and $\mathbf{I}_{backgr}$. Furthermore the intensities are assumed to be measured with Poisson distribution such that the variance is equal to the value of the quantities.

The optimal $\boldsymbol{\eta}^{theory}$ is selected as the model having minimum reduced χ^2, $\min_{\boldsymbol{\eta}^{theory} \in database} \chi^2$.

The found model is accepted if following criteria are fulfilled

- The reduced χ^2 value is within the specified confidence levels predicted by the χ^2-distribution
- The parameters are linear independent[4]

3. SAMPLES

3.1. Binary Photoresist gratings

The, photoresist grating on glass, samples were manufactured using near-field (NFH) printing technique. The principle of the NFH technique is the use of a phase mask capable of diffracting an incoming light beam into two transmitted beams of different orders (0^{th} and -1^{st}) and equal magnitude. Interference between these beams creates an intensity

pattern with a period equal to the period of the phase mask[9]. The generated intensity pattern is exposed to the photoresist that is subsequently developed leaving a resist grating mask.
The NFH-printing was conducted using a modified mask aligner, MA4, from SUSS equipped with a traditional mercury arc lamp, collimating lenses, 365 nm narrow band filter, and phase mask of 318 nm (or 360 nm) period[10]. The light was incident on the phase mask at the Bragg angle of 35.0° (or 30.5°).
The presence of the substrate below the phase mask induces additional interference patterns in the photoresist created by superposition of the reflected light from the substrate and the diffracted light. These patterns have other periods than the intensity pattern originated from interference between the non-reflective beams and hence degrade the quality of the printing quality of the grating. A solution to this particular problem is applying top anti-reflective coating (TARC) for additional minimization of reflections. The materials applied in this work were a positive photoresist, AZ1518, and a TARC, Aquatar, both from Clariant, and glass substrates AF45 of thickness 0.70 mm from Scott.
Figure 3 shows the calculated reflectance from a TARC-resist-glass layered structure. The optimal layer thickness is approximately 165 nm resist and 68 nm TARC resulting in reflections less than 0.5%. The optimal layer thickness was experimentally confirmed.
Six glass substrates were spun with AZ1518 photoresist followed by annealing at 90°C for 30 min in nitrogen atmosphere and afterwards spun with TARC Aquatar.
The samples were exposed to different energy density levels and subsequently developed. The period of the NFH phase masks and applied energy densities are summarized in Table 2

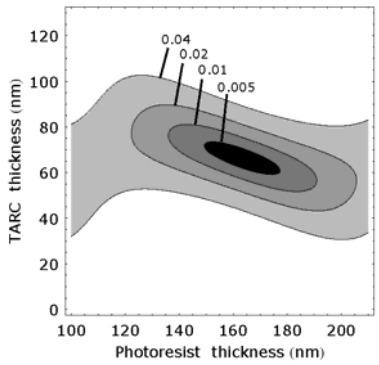

Figure 3: Contour plot showing the calculated reflectance of the TARC-photoresist-glass layered structure as function of layer thicknesses using illumination at 365 nm at an illumination angle of 35.0° (optimum for the 360 nm grating NFH-printing). The absolute reflection levels are indicated in the plot.

3.1.1. Simplified Resist Grating Model

A simple model for recording grating pattern in thin photoresist layer assumes, that the thickness of the photoresist remaining after development, is given by the delivered exposure energy density. For positive photoresist increased exposures leads to thinner photoresist layers.
We have assumed an analytical function describing the photoresist thickness as function of delivered energy density where the remaining thickness of photoresist normalized to the initial thickness is expressed by

$$C(W) = \begin{cases} \tanh\left(\gamma(1-W)\right) & W < 1 \\ 0 & \text{otherwise} \end{cases}$$

W is the exposure energy density normalized to the minimum required energy density for complete removal of photoresist, i.e. 'dose-to-clear' is obtained for W=1. The curve is denoted the characteristic curve and the parameter γ, that is the absolute slope of the characteristic curve at dose-to-clear W=1, is called the contrast constant[11]. Figure 4 shows examples of the modeled characteristic curve. The contrast constant γ is used as a fitting parameter.

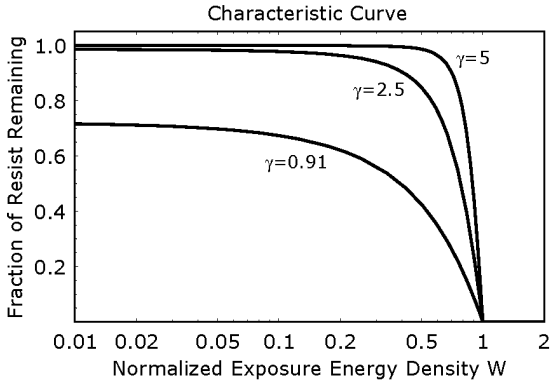

Figure 4**:** Plot of the characteristic curves applied in the modeling for various contrast constants γ .

The delivered exposure energy density in the photoresist layer in a typical NFH-printing is sinusoidal along the repeated direction *x* with period Λ . This is expressed as

$$W(x) = W_0 \sin^2(\pi \tfrac{x}{\Lambda})$$

where W_0 is the exposure energy density delivered to the NFH phase mask.

Substitution of the sinusoidal energy density pattern into the expression for the characteristic curve $C(W)$ results in an analytical profile function of the NFH-printed photoresist,

$$z(x,\boldsymbol{\alpha}) = h_0 C\left(W(x)\right) = \begin{cases} h_0 \tanh\left(\gamma\left(1 - W_0 \sin^2(\pi \tfrac{x}{\Lambda})\right)\right) & W_0 < 1 \\ 0 & \text{otherwise.} \end{cases}$$

where the profile parameter $\boldsymbol{\alpha} = (h_0, W_0, \gamma)$ contains the process parameters, delivered exposure energy density W_0, contrast constant γ and initial (pre-exposure) layer thickness of photoresist h_0.

Figure 5 shows examples of modeled photoresist profiles for different exposure levels.

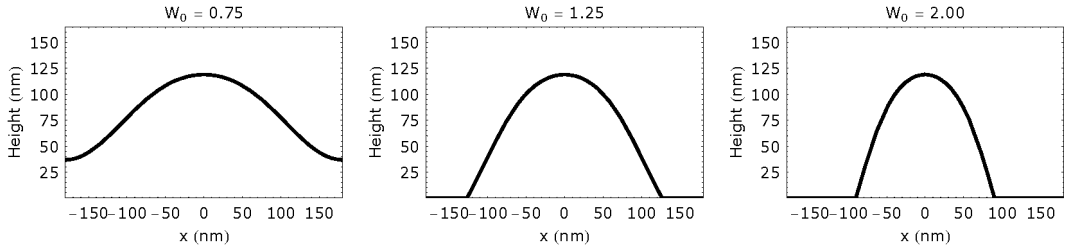

Figure 5: Plot of cross-sectional photoresist profiles generated by the herein simple analytical model for various exposure energy densities W_0. Following values were used for the calculation: initial resist layer thickness h_0 = 165 nm, the period of the modulated exposure light Λ = 360 nm and the contrast constant of the resist γ = 0.91.

However, it is useful to recast the profile parameters into geometrical quantities including height, bottom width and effective duty cycle. The quantities are defined below for two cases. The first case describes profile shapes having regions with complete removal of photoresist, i.e. the exposure level have exceeded $W_0 > 1$. In the other case, $W_0 < 1$, a sinusoidal photoresist profile is formed without regions of complete photoresist removal. We obtain the following expression:

	Symbol	$W_0 > 1$	$W_0 < 1$
Profile height (top-to-bottom distance)	h	$h_0 \tanh\gamma$	$h_0\left[\tanh\gamma - \tanh\left(\gamma(1-W_0)\right)\right]$
Bottom width	w_b	$2\frac{\Lambda}{\pi}\arcsin(\frac{1}{\sqrt{W_0}})$	N/A
Effective duty cycle	f	$\frac{1}{h\Lambda}\int z(x)dx$	$\frac{1}{h\Lambda}\int\left(z(x,\boldsymbol{\alpha}) - h_0\tanh\left(\gamma(1-W_0)\right)\right)dx$

This photoresist model is applied in the ODM analysis and uses a lookup table generated from the initial layer thickness of resist h_0 and delivered exposure energy density W_0. The contrast constant γ used herein was found by searching for best least-square fit between measured ODM data and modeled ODM data for all the gratings simultaneously. The best result was a contrast constant at γ=0.91.

3.2. Multi-layer sub-micron gratings

A single multi-layer surface relief reflection grating has been investigated. The grating is of the resonant type[12] consisting of a dielectric mirror (alternating Ta_2O_5-SiO_2 quarter-wave layers) and a corrugated surface. The grating of period 560 nm was printed by recording a 442 nm interferogram into a thin photoresist layer spin-coated onto the multi-layer. The photoresist grating pattern was then physically transferred into the last Ta_2O_5 layer by inductively coupled plasma reactive ion etching (ICP-RIE). See Table 1 for details. Such resonant grating was shown to give rise to more than 99% diffraction efficiency for the -1^{st} order due to the fulfillment of the leaky mode resonance condition in the mirrored corrugated dielectric slab[13]. Figure 6 shows the eleven measurement regions, which have been investigated using AFM and ODM.

Fab3		
Layer number	Material	Thickness [nm]
20	Ta_2O_5	70
19	SiO_2	152
18	Ta_2O_5	131
17	SiO_2	223
16	Ta_2O_5	131
15	SiO_2	223
14	Ta_2O_5	131
⋮	⋮	⋮
5	SiO_2	223
4	$Ta2O_5$	131
3	SiO_2	223
2	Ta_2O_5	131
1	SiO_2	223

Table 1: Deposited homogeneous layers on a quartz substrate. Layer number 20 is the corrugated layer at the air side.

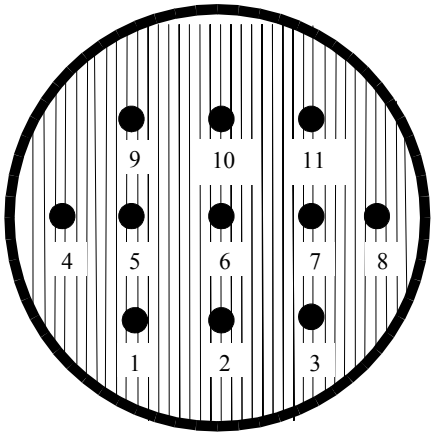

Figure 6: Locations of measured point on sample Fab3.

4. RESULTS

4.1. Experimental Setup

The ODM measurements were conducted for normal incidence with a beam diameter of 0.20 mm. The data analysis is based on the transmitted zero-order diffraction efficiency since the measured high-order diffraction ratio spectrum showed that the structure were symmetrical. In the reconstruction of the grating profiles the period Λ of all samples was known and therefore not assessed by the ODM analysis.

4.2. Binary Photoresist grating

The profile of the developed resist grating was investigated using ODM and Atomic Force Microscopy (AFM). The ODM measurements were carried out using TM polarization.
The results of the measurements on the photoresist gratings are summarized in Table 2 and Table 3. It is seen that there is a good agreement between ODM and AFM height measurements and that the duty cycle and bottom width found by AFM is systematically higher than the corresponding ODM measurements. This is clearly seen by comparison of the ODM and AFM measured profiles shown in Figure 7 and Figure 8. The discrepancy between the AFM and ODM duty cycle (and bottom width) results is likely to arise from the convolution of the AFM stylus shape into the profile of the grating.
Figure 7 shows a plot of the modeled and measured ODM efficiency data demonstrating a very good fit, which also is confirmed by the value of the reduced χ^2. Figure 8 shows an image of the photoresist grating S3 measured by AFM.

Sample	Experimental parameters		Measured ODM quantities			
	Period Λ	Delivered exposure energy density	Normalized exposure energy density	Pre-expose height	Reduced χ^2 @ optimum fit	Comment
	(nm)	[mJcm^{-2}]		[nm]		
B1	360	150	0.93	135.1	2.75	Lines in contact
B11	360	225	1.45	159.9	2.75	Separated lines
B19	360	375	2.65	155.0	0.72	
S1	360	200	1.18	160.0	2.26	
S2	360	450	2.90	145.0	1.99	
S3	318	300	2.33	175.0	1.35	

Table 2: Measured ODM results of the set of photoresist gratings. The fitted process parameters, normalized exposure energy density, W_0, and pre-exposure height, h_0, of the developed photoresist grating are listed for the different delivered energy densities. The exposure energy density and printed grating period, Λ, applied in the sample preparation are included.

Sample	ODM			AFM		
	h	w_b	f	h	w_b	f
	[nm]	[nm]		[nm]	[nm]	
B1	97	N/A	0.54	109		
B11	115	225	0.42	129		
B19	112	152	0.29	118		
S1	115	268	0.48	128 (3)	NA	0.49 (0.04)
S2	105	144	0.28	102 (3)	186 (15)	0.36 (0.04)
S3	126	145	0.31	129 (3)	184 (15)	0.36 (0.04)

Table 3: Measured ODM and comparative AFM results of the set of photoresist gratings. The fitted parameters from Table 2 is converted to the geometrical quantities profile height, h, profile bottom width, w_b, and effective duty cycle f. The numbers in parenthesis are the standard uncertainties corresponding to a coverage probability of 68%.

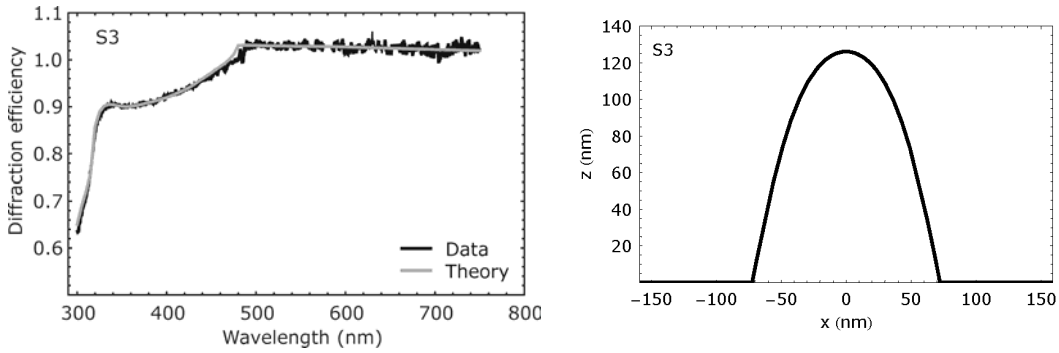

Figure 7: Left sided plot shows the ODM measurement of grating S3 and the best fitted spectra. Right side shows the cross-sectional photoresist grating profiles corresponding to the best fitted spectra.

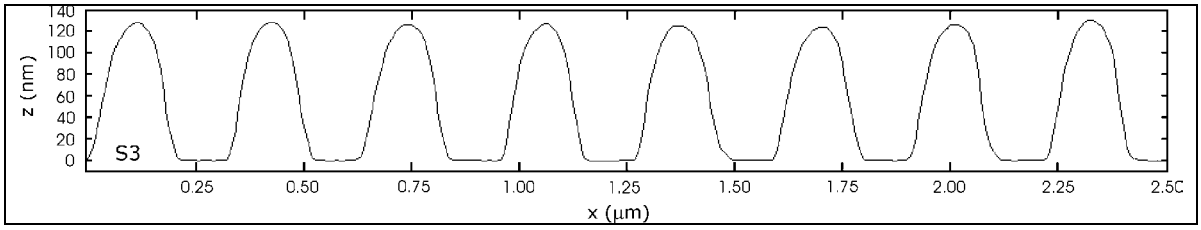

Figure 8: Image of the sample S3 the image is an average profile of the measured AFM image. The profiles are not corrected for AFM stylus convolution.

4.3. Multi-layer sub-micron grating

The zero-order diffraction efficiency for the TE polarization including the best fit to the data obtained by ODM using a rectangular profile is shown in Figure 9. A good agreement between theory and experimental data is seen from the plot. In Table 4 the found values for all measurement points are summarized. It is seen that there is a good agreement between ODM and AFM height measurements and that the duty cycle obtained by AFM is higher than the corresponding ODM measurements for all measured locations with the exception of point 4 and 8, which are located close to the rim of the sample. The differences between the AFM and ODM measured duty cycle at the centre sample area are expected as no deconvolution of the stylus shape has been performed, whereas the difference at the sample rim indicates that the grating is inhomogeneous at the rim.

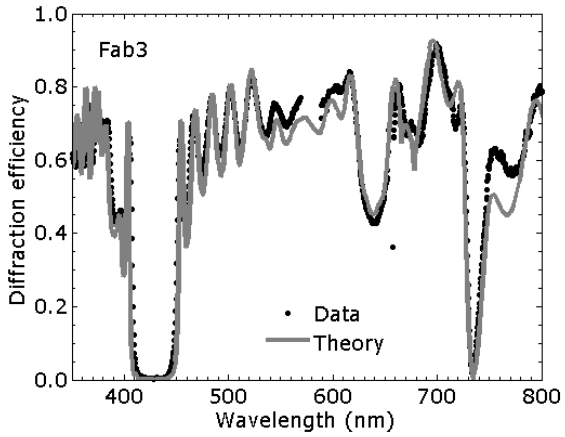

Figure 9: Measured and modeled zero-order diffraction efficiency of the multi-layer grating. Experimental data between 570 nm and 590 nm has been excluded due to saturation of the spectrometer at these wavelengths.

Measurement point location	ODM height	AFM height	ODM duty cycle	AFM duty cycle
	[nm]	[nm]	%	
1	49.9	52.3	38	43.8
2	49.0	52.2	39	42.9
3	50.9	52.1	34	38.4
4	54.8	50.7	97	54.5
5	51.4	53.7	35	40.2
6	50.5	54.2	38	41.1
7	51.9	54.7	32	35.7
8	45.3	51.3	25	35.7
9	51.1	51.8	35	42.0
10	50.3	52.8	38	44.6
11	51.6	52.2	34	36.6

Table 4: Comparison between results from the ODM and AFM measurements of the multi-layer grating obtained at the point locations described in Figure 6.

5. Conclusion

In conclusion we find that both the ODM measurements have succeeded in giving the *complete* profile with nanometer scale accuracy and that the results are in very good agreement with AFM measurements of the heights. We have thus demonstrate that the ODM is capable of determining grating profile parameters and photoresist exposure levels. In earlier work[4, 14] we demonstrated that ODM is also capable of measuring the grating profile of high aspect ratio sub micron gratings with period ranging from 220 nm to 1000 nm. In conclusion we have demonstrated that the ODM is a versatile tool for grating profile characterization.

6. Acknowledgement

We would like to acknowledge for the financial support from the Ministry of Science, Technology and Innovation under contract CEMOST 2002-603/4001-97/55118. The multi-layer grating characterization is part of a round robin within Network of Excellence NEMO.

REFERENCES

1. E. N. Glytsis, Two-dimensionally-periodic diffractive optical elements: Limitations of scalar analysis, J. Opt. Soc. Am. A **19** pp 702-715, 2002.
2. D. A. Pommet, M. G. Moharam and E. B. Grann, Limits of scalar diffraction theory for diffractive phase elements, J. Opt. Soc. Am. A **11** pp 1827-1834, 1994.
3. T. O. Korner, J. T. Sheridan and J. Schwider, Interferometric resolution examined by means of electromagnetic theory, J. Opt. Soc. Am. A **12** pp 752-761, 1995.
4. J. Garnæs, P.-E. Hansen, N. Agersnap, J. Holm, F. Borsetto and A. Kühle, Profiles of high aspect ratio grating determined by optical diffraction microscopy and atomic force microscopy, submitted to Applied Optic, 2005.
5. Patent WO2004008069 (Niels Agersnap Larsen and Poul-Erik Hansen, Method and apparatus for optically measuring the topography of nearly planar periodic structures, July 2002).
6. L. Li, New formulation of the Fourier modal method for crossed surface-relief gratings, J. Opt. Soc. Am. A **14** pp 2758-2767, 1997.
7. M. G. Moharam, D. A. Pommet, E. B. Grann and T. K. Gaylord, Stable implementation of the rigorous coupled-wave analysis for surface relief gratings: Enhanced transmittance matrix approach, J. Opt. Soc. Am. A **12** pp 1077-1086, 1995.
8. L. Li, Fourier modal method for crossed anisotropic gratings with arbitrary permittivity and permeability tensors, J. Opt. A: Pure Appl. Opt. **5** pp 345-355, 2003.
9. D. M. Tennant, T. L. Koch, P. P. Mulgrew, R. P. Gnall, F. Ostermeyer, and J.-M. Verdiell, Characterization of near field holography grating masks for optoelectronics fabricated by electron beam lithography, J. Vac. Sci. Technol. B **10**, no. 6, pp. 2530–2535, 1992.
10. IBSEN Photonics, Ryttermarken 15-21, DK-3520 Farum, Denmark. URL: www.ibsen.dk.
11. H. J. Levinson, Principle of lithography, SPIE Press, 2001.
12. A.V. Tishchenko, V.A. Sychugov, High grating efficiency by energy accumulation in a leaky mode, Opt. and Quantum Electron., **32,** pp. 1027-1031, 2000.
13. N. Destouches, A.V. Tishchenko, J.C. Pommier, S. Reynaud, O. Parriaux, 99% efficiency measured in the -1^{st} order of a resonant grating, Optics Express, **13**, pp. 3230-3235, 2005.
14. J. Garnæs, P.-E. Hansen, N. Agersnap, I. Davi, J.C. Petersen, A. Kühle, J. Holm and L. H. Christensen, Determination of sub-micrometer high aspect ratio grating profiles, Proc. SPIE, Vol. 5378, Advanced Characterization techniques for optics 2005, semiconducters, and Nanotechnologies II, San Diego, California, USA, 31 July - 4 August 2005. In preparation.